View metadata, citation and similar papers at core.ac.uk

brought to you by CORE

provided by International Journal of Computer (IJC - Global Society of Scientific Research and...

International Journal of Computer

(IJC)

ISSN 2307-4523 (Print & Online)

© *Global Society of Scientific Research and Researchers*

http://ijcjournal.org/

Hough Transform and Chi-Square-Based Iris Recognition

Olabode Olatubosun[a], Iwasokun Gabriel Babatunde[b]*, Oluwadare Samuel Adebayo[c], Adeniyi Tunde Taiwo[d]

[a,b,c,d] *Federal University of Technology, Akure, Nigeria*

[a]*Email: oolabode@futa.edu.ng*

[z]*Email: gbiwasokun@futa.edu.ng*

[c]*Email: ttadeniyi@futa.edu.ng*

Abstract

The paper proposes a new iris recognition method based on canny edge detection, Hough transform, pseudo-polar coordinate, wavelet transform and chi-square algorithms. The iris image is firstly converted to greyscale before the edge detection, segmentation, normalization, feature extraction and feature matching operations are performed in sequential order. Feature extraction module uses wavelet transform-based approach to extract standard iris features while the feature matching module relies on chi square algorithm for reference and template-based feature matching. Analyses of the experimental results revealed satisfactory performance of the new method and its dependence on the quality of the hardware used for image acquisition. Comparison of obtained results with those from some existing iris recognition systems showed competitiveness and superiority of the new method.

Keywords: Iris recognition; Hough transform; chi square; security.

1. Introduction

The traditional human identity management methods, which include possession (such as identity and smart cards) and knowledge (such as Personal Identification Number (PIN) and password)-based human identification schemes suffer various limitations that include theft, forgery, unauthorized access and forgetfulness. Several private and public organizations have considered strengthening their knowledge-based security systems with longer and dynamic (changing) passwords, which require individuals documenting their passwords in unsecured manners.

---

* Corresponding author.

The compromise of a re-used password on different systems may lead to theft, privacy intrusion and other consequences [1]. Biometric-based automated personal identification has received considerable attention in the last decade as a solution to these problems [2]. All the physiological biometrics are related to the shape of the body, naturally endowed and include fingerprint, palm print, hand geometry, iris, face, scent/odor, Deoxyribonucleic Acid (DNA) and nose. A behavioral biometric is formed based on the pattern of behavior of a person and examples include handwriting (typing rhythm), signature, gait and voice [3]. The high confidence and success levels recorded for biometric-based systems have been attributed to strict and direct covert observation of information, non-sharability, not-transferable and regeneration within short period when damaged or mutilated. In addition, biometrics-based systems are very easy to use, friendly and repudiation-proof [4].

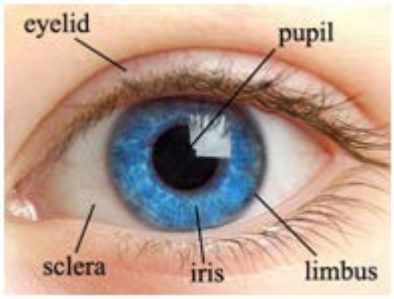

Figure 1: An iris and its main components

The iris (shown in Figure 1) is a physiological biometric and represents the portion of the eye that surrounds the pupil and is fully rich in colored and textual patterns that are distinct for left and right eyes and for individuals [5]. It consists of distinct characteristics such as the freckles, coronas, strips, furrows and so on [6]. It is sandwiched between the white sclera and the pupil (which is the black image) and it begins to form in the third month of gestation. The structures creating iris pattern are largely completed in the eight months while the pigment accretion continues in the first postnatal years. An iris contains many distinctive and visible features (often called the texture) such as arching ligaments, furrows, ridges, crypts, rings corona, freckles and zigzag collaret which are unique to each subject [7]. Iris recognition is one of the most reliable and accurate biometric identification schemes due to its very high level of uniqueness, accuracy and stability [2, 8-9]. An iris recognition system is often divided into preprocessing, segmentation, normalization, feature extraction and matching phases. The pre-processing phase is used to convert the image to grayscale and remove associated noise. Segmentation is used to separate the iris region from the entire grayscale image while normalization is used to fix the dimensions of the segmented iris region to allow for accurate comparisons. The feature extraction and the matching phases perform the extraction of the biometric templates (which form the iris signature or the feature vector) from the normalized image and the matching of the template and reference images respectively. The high precision of each of these phases is very essential for a good performance of an iris system [10].

The existing iris matching algorithms include Circular Hough Transform (CHT) [10], Haarlet Pyramid [9],

Local Invariant Feature Descriptor [2], Multi-scale Taylor Expansion [11], Wavelet Packet Decomposition [2, 12], Edge Detection/Gaussian Filter [13] and Dichotomy Model [14]. Although several of these algorithms show promising results for segmentation, normalization and feature extraction, there is a common problem of high acceptance and rejection rates for multiple images of the same subject. This paper reports on the formulation and implementation of a 2D wavelet and chi-square-based iris recognition model which provides reasonable solution to this problem.

2. Literature Review

The authors in [15] proposed a new iris coding procedure based on non-reversible Zak-Gabor wavelet packet transform. The procedure allows the selection of the between-to-within class ratio, frequency and scale that are appropriate for image transformation in terms of the system reliability to the given iris image quality and resolution. In [16], an algorithm for iris feature extraction based on 2D Haar wavelet is proposed. The iris is firstly decomposed by the 2D Haar wavelet to form a 375-bit code based on quantizing of all the high-frequency coefficients. The matching scheme is based on similarity degree function. The authors in [17] proposed a video camera and frame grabber-based system for capturing an iris image and the extraction of its feature based on wavelet transforms. The system successfully captured and recognized iris images but its hardware design lacks the strength for producing optimal image quality due to constraints on type, lighting and distance of the camera. Methods for iris feature subset selection and vector creation are proposed in [18]. Contourlet Transform Technique (CTT), which captures the intrinsic geometrical structures of an iris image, is used to extract deterministic feature sequence. The iris image is decomposed into a set of directional sub-bands with texture details captured in different orientations at various scales to reduce the feature vector dimensions. Support Vector Machine (SVM) classifier is also used for the approximation of the identification.

In [19], a non-cooperative Gabor descriptor-based iris recognition algorithm in which feature extraction and comparison are scale, deformation, rotation and contrast-invariant-based is proposed. Gabor wavelet is incorporated with Scale-Invariant Feature Transformation (SIFT) to obtain a reliable extraction of features. The algorithm performs well with off-angle and low resolution iris images but needs further improvement for iris images with multiple angle enrolment. The authors in [20] presented a Haar wavelet packet-based iris recognition system that significantly decreases the error rates. Though the system is suitable for application within non cooperative images, it experiences high degradation with noisy images. The authors in [21-22] presented two-dimensional complex wavelet transform (2D-CWT)-based methods for iris recognition. 2D-CWT does not only keep wavelet transform's properties of multi-resolution decomposition analysis and perfect reconstruction; it also approximates shift invariance and offers good directional selectivity for 2-D image with limited redundancy in iris feature extraction. It also localizes the circular iris and pupil region, occluding eyelids and eyelashes and reflections. The extracted iris region was normalized into a rectangular block with constant dimensions to account for imaging inconsistencies. The phase information of the coefficients was used for feature encoding. While He and Shi adopted Hamming distance for classification, Singh and Gangrade extracted and quantized data to four levels with a view to encoding the unique pattern of the iris into a bit-wise biometric template and performed classification of iris templates based on K-nearest neighbor technique. Though the methods reduce the computational cost and improve the classification accuracy, their performance

is strictly dependent on the directional and selective property of CWT.

The authors in [23] presented a Wavelet Packet Analysis (WPA) and Morlet wavelet-based platform for iris recognition. Morlet wavelet offered trivial computations compared to Gabor wavelets. The visible texture of a person's iris is encoded into a compact sequence of 2-D Morlet wavelet coefficients, which generate iris codes that are compared based on XOR logic. Though the platform simplifies computation with less complexity, it experiences low accuracy rates. The authors in [6] presented an iris recognition system with four steps; namely image segmentation using Canny Edge Detector, Circular Hough Transformation (CHT) for iris and pupil localization and normalization, feature extraction using discrete 2D reverse bi-orthogonal wavelet and iris codes comparison. Though the system offers a high recognition rate, accuracy of the results is dependent on the effectiveness of the segmentation and normalization algorithms. In [24], an algorithm for finding the most efficient multi-wavelet family and its coefficients for encoding iris templates for experimental samples is proposed. The algorithm performs segmentation, normalization, feature encoding and matching by using series of Multi-wavelet families. Feature encoding is based on decomposition of the normalized iris image. The system achieves higher recognition efficiency and robustness but experiences computational complexities.

3. Proposed Algorithm

The algorithm is conceptualized in Figure 2 with edge detection, segmentation, normalization, feature extraction and feature matching as its major steps.

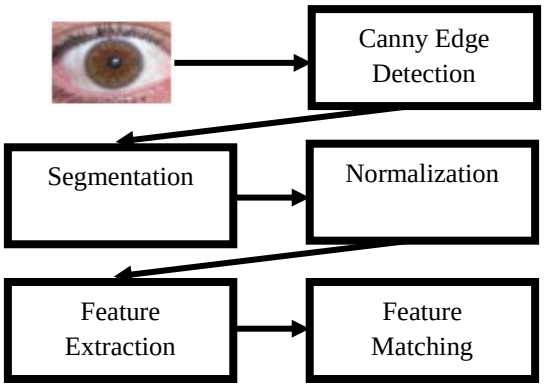

Figure 2: Steps of the proposed algorithm

3.1 Canny Edge Detection

Edge detection is an important part of perception process [25-27] and its major aim is to find local discontinuities which are of interest in some image attributes such as intensity or color. These discontinuities are of interest because they are likely to occur at the boundaries of objects where local edges may also occur due to variations in surface characteristics and changes in illumination. Canny edge detector algorithm is used to find the edges by separating noise from input image and contains a number of adjustable parameters which promote its effectiveness and reduction in the computation time with distortion-free feature extraction [25]. The

algorithm involves capturing of the intuitive criteria which are given in readily readable and solvable mathematical forms. Given that $f(x)$ and $G(x)$ denote the impulse response of the filter and the edge respectively, then with the edge centered at $x = 0$, the response of the filter at center H_G is given by a convolution integral [28]:

$$H_G = \int_{-W}^{+W} G(-x)f(x)dx \tag{2}$$

[- W, W] is the finite impulse response and the root-mean-squared response to the noise $n(x)$ only, is computed from:

$$H_n = {n_0}^2 \left[\int_{-W}^{+W} G(-x)f(x)dx \right]^{1/2} \tag{3}$$

n_0^2 is the mean-squared noise amplitude per unit length. For the first criterion, the output signal-to-noise ratio (SNR) is the quotient of the two responses and is expressed as follows:

$$SNR = \frac{\left| \int_{-w}^{+w} G(-x)f(x)dx \right|}{n_0 \sqrt{\int_{-w}^{+w} f^2(x)dx}} \tag{4}$$

Let $H_n(x)$ be the response of the filter to noise only, and $H_G(x)$ be its response to the edge, and suppose there is a local maximum in the total response at the point where $x = x_0$, then:

$$H_n'(x_0) + H_G'(x_0) = 0 \tag{5}$$

The Taylor expansion of $H_G'(x_0)$ about the origin gives:

$$H_G'(x_0) = H_G'(0) + H_G''(0)x_0 + O(x_0^2) \tag{6}$$

Base on assumption, $H_G'(0) = 0$, which implies the response of the filter in the absence of noise has a local maximum at the origin, so the first term in the expansion is ignorable and therefore, Equations (5) produces:

$$H_G'(0)x_0 \approx -H_n'(x_0) \tag{7}$$

$H_n'(x_0)$ is a Gaussian random quantity whose variance is the mean-squared value of $H_n'(x_0)$, and is derived from:

$$E[H_n'(x_0)^2] = n_0^2 \int_{-w}^{+w} f'^2 x dx \tag{8}$$

$E[y]$ produces the expected value of y which combines with Equation (7) while substituting for $H_G''(0)$ to give:

$$E[x_0^2] \approx \frac{n_0^2 \int_{-w}^{+w} f'^2 x dx}{\left[\int_{-w}^{+w} G'(-x) f'(x)\, dx\right]^2} = \delta x_0^2 \tag{9}$$

δx_0 is an approximation to the standard deviation of x_0. The localization, l is defined as the reciprocal of δx_0.

$$l = \frac{\left|\int_{-W}^{+W} G'(-x) f'(x) dx\right|}{n_0 \sqrt{\int_{-W}^{+W} f'^2(x) dx}} \tag{10}$$

Equations (4) and (10) are mathematical forms for the first two criteria, and the design problem simultaneously reduces to their maximization. It is therefore important to maximize the product of of the two equations by using the product function to simplify the analysis for step edges as follows:

$$\frac{\left|\int_{-w}^{+w} G(-x) f(x) dx\right|}{n_0 \sqrt{\int_{-w}^{+w} f^2(x) dx}} \frac{\left|\int_{-w}^{+w} G'(-x) f'(x) dx\right|}{n_0 \sqrt{\int_{-w}^{+w} f'^2(x) dx}} \tag{11}$$

The SNR and localization criteria can be trivially maximized based on Schwarz inequality as shown in Equations 12 and Equation 13, respectively.

$$n_0^{-1} \int_{-w}^{+w} G^2(x) dx \tag{12}$$

$$n_0^{-1} \int_{-w}^{+w} G'^2(x) dx \tag{13}$$

The distance between adjacent maxima in the noise response of f, denoted by x_{max}, will be $2X_{zc}$ and this distance is set to k, which is a fraction of the operator width, W and fixes the number of noise maxima that could lead to a false response. The response of the filter will be concentrated in a region of width 2W, and the expected number of noise maxima, N_n in this region is obtained from:

$$N_n = \frac{2W}{x_{max}} = \frac{2}{k} \tag{14}$$

3.2 Detection for step edges

If the results of the last section are specialized to the case where the input $G(x)$ is a step edge and given that $G(x) = Au_{-1}(x)$ where $u_n(x)$ is the nth derivative of a delta function and A is the amplitude of the step, then:

$$u_{-1}(x) = \begin{cases} 0, & for\ x < 0; \\ 1, & for\ x \geq 0; \end{cases} \tag{15}$$

Substituting for $G(x)$ in Equations (4) and (10) gives:

$$SNR = \frac{A\left|\int_{-w}^{0} f(x)dx\right|}{n_0\sqrt{\int_{-w}^{+w} f^2(x)dx}} \tag{16}$$

$$l = \frac{A|f'(0)|}{n_0\sqrt{\int_{-w}^{+w} f'^2(x)dx}} \tag{17}$$

Removing this dependence on the image and defining two performance measures ∑ and Λ which strictly depend on the filter gives:

$$SNR = \frac{A}{n_0}\Sigma(\mathrm{f})\ \Sigma(\mathrm{f}) = \frac{\left|\int_{-w}^{0} f(x)dx\right|}{\sqrt{\int_{-w}^{+w} f^2(x)dx}} \tag{18}$$

$$l = \frac{A}{n_0}\Lambda(f')\ \ \Lambda(f') = \frac{f'(0)}{\sqrt{\int_{-w}^{+w} f'^2(x)dx}} \tag{19}$$

Substituting f_w into Equations (18) and (19), the performance of the scaled filter is obtained as follows:

$$\Sigma(f_w) = \sqrt{w\Sigma(\mathrm{f})} \qquad and \qquad \Lambda\left(f'_w\right) = \tfrac{1}{\sqrt{w}}\Lambda(f') \tag{20}$$

Since this product would be invariant under changes in scale, then:

$$\Sigma(f)\Lambda(f') = \frac{\int_{-w}^{0} f(x)dx}{\sqrt{\int_{-w}^{+w} f^2(x)dx}}\ \frac{|f'(0)|}{\sqrt{\int_{-w}^{+w} f'^2(x)dx}} \tag{21}$$

The solutions to the maximization of this expression will be a class of functions all related by spatial scaling and independent of the method of combination of the criteria.

3.3 Segmentation

Segmentation based on Hough Transform (HT) is used to mark the iris and the pupil boundaries and to remove the eyelid [29]. HT is described as a transformation of a point in a 2-dimensional region to a shape-dependent parameter space. It provides an established method for shape recognition in digital images, straight lines, circles, ellipse and other arbitrarily shaped objects. It offers high robustness to noise and shape distortions and provides occlusions to the effects of missing parts of an object. However, its computation and storage requirements increase as a power of the dimensionality of the curve [30]. The basic functionality of the HT is a straight line in the x, y-plane described by [31]:

$$y = m * x + b \tag{27}$$

The line is represented in the Cartesian coordinate system by the intercept, b and slope, m and due to the offer of unbounded values for parameters m and b by the perpendicular lines to the x-axis, lines are parameterized in terms of theta θ and r such that:

$$r = x * cos(\theta) + y * sin(\theta), \text{ for } \theta \in [0, \pi] \quad (28)$$

r is the distance between the line and the origin, θ is the angle. Every line passing through point (x, y) can uniquely be represented by (θ, r) with θ and r (which have the maximum value of two times the diagonal of the image) assuming finite sizes. Equation (28) corresponds to a sinusoid curve in the (r, θ) plane and it is unique to point [x, y]. Sinusoids crossing arise if multiple points are located on the same line. The result of segmentation is the region of interest on which cropping is applied to get rid of unwanted regions.

3.4 Normalization

Normalization is used to remove the effect of illumination and other factors. Robust representations for iris recognition must be resistant to changes in size, position and orientation of the patterns. With iris recognition, this implies a mandatory creation of a representation that is invariant to the optical size of the image and the location of the iris within the image. For rotated iris images, a projected pseudo polar coordinate system (PPCS) which can be described as doubly-dimensionless with polar variable and angle is used. PPCS is inherently dimensionless due to its ranging from the pupillary boundary to the limbus within the interval [0, 1] [32]. The dilation and constriction of the elastic meshwork of the iris when the pupil changes size is intrinsically modeled by the coordinate system to give the stretching of a dissimilar rubber sheet with the topology of an annulus anchored along its outer perimeter and tension controlled by an (off-centered) interior ring of variable radius. The dissimilar rubber sheet model gives a pair of real coordinates $(r;\ \theta)$ to each point on the iris (regardless of size and pupillary dilation) while r is on the unit interval $[0, 1]$ and θ is the angle in the interval $[0, 2\pi]$. The re-mapping of the iris image $I(x, y)$ from the raw Cartesian coordinates (x, y) to the dimensionless non-concentric polar coordinate system (r, θ) is represented by [3]:

$$I\big(x(r,\theta), y(r,\theta)\big) \rightarrow I(r,\theta) \quad (29)$$

$$x(r,\theta) = (1-r)x_p(\theta) + rx_i(\theta) \quad (30)$$

$$y(r,\theta) = (1-r)y_p(\theta) + ry_i(\theta) \quad (31)$$

(x_p, y_p) and (x_i, y_i) give the pupil and iris coordinates, respectively along θ direction.

3.5 Features Extraction

A wavelet transform-based feature extraction was performed on every iris image to form a unique and ordered sequence of its signature. Wavelet transform provides information about the scale and characteristics shape of the wavelet and is defined as follows:

$$\psi(x) = \begin{cases} -1 & x \in [0, \frac{1}{2}) \\ 1 & x \in (\frac{1}{2}, 1] \\ 0 & o/\omega \end{cases} \tag{32}$$

Given a wavelet, $\psi(x)$ the coefficients (for a required level 2^j and for $k \in \{1, \dots, j\}$) is obtained from:

$$d_{j,k} = \int f(x)\psi_{j,k}(x)dx \tag{33}$$

Based on the combination of $c_{j,k}$ and $d_{j,k}$, all the required coefficients are calculated and the decomposition of the original function is performed as follows:

$$f(x) = \sum_{j,k} d_{j,k}\, \psi_{j,k}(x) \tag{34}$$

By implication, a function f(x) can be represented as a linear combination of scaling of a single basis function such that for all x, the wavelets satisfy the following dilation equations:

$$\psi(x) = \sum_{k} g_k\, \psi(2x - k) \tag{35}$$

$$\phi(x) = \sum_{k} h_k\, \phi(2x - k) \tag{36}$$

The whole set of wavelets are characterized by a suitable choice of h_k (low pass) and g_k (high pass) quadrature mirror filters which define discrete wavelets and serve as link between the wavelets as follows:

$$\psi(x) = \sum_{k} g_k \sqrt{2}\, \psi(2x - k) \tag{37}$$

$$\phi(x) = \sum_{k} h_k \sqrt{2}\, \phi(2x - k) \tag{38}$$

The associated discrete wavelets ϕ_j are vectors of length $L_j = (2^j - 1)(N_h - 1) + 1$ (where N_h is the number of non-zero elements of $\{h_k\}$) whose elements are from:

$$\phi_{1,n} = \sum_{k} h_{n-2k}\delta_{0,k} = h_n \quad for\ n = 0, \dots, L_1 - 1 \tag{39}$$

$$\phi_{(j+1),n} = \sum_k h_{n-2k}\phi_{j,k} \quad for\ n = 0, \dots, L_1 - 1 \tag{40}$$

The discrete wavelets ψ_j are also defined in the same way using $\{g_k\}$ instead of $\{h_k\}$.

Prior to the introduction of two-dimensional wavelets, outer products are used to combine the vectors to form a scalar while outer products are used to extrapolate them. Given two vectors **a** and **b** of length n and m respectively, then the standard outer product, ⊗ is defined as follows:

$$\boldsymbol{a}\otimes\boldsymbol{b} = \boldsymbol{a}\boldsymbol{b}^{\boldsymbol{T}} = C \tag{41}$$

Where C is a matrix with elements defined by:

$$C_{i,j} = a_i \text{ x } b_j \tag{42}$$

The concept of outer products is then used to define two-dimensional discrete wavelets by taking the outer products of one-dimensional wavelets $\psi_{j,k}$ and $\phi_{j,k}$ as follows:

:

$$\psi_j^h = \phi_j \otimes \psi_j \tag{43}$$

$$\psi_j^v = \psi_j \otimes \phi_j \tag{44}$$

$$\psi_j^d = \psi_j \otimes \psi_j \tag{45}$$

3.6 Iris Matching

For the template and reference features, I and J, the system computes the matching score D(I, J) based on the formula:

$$D(I,J) = \sum_{i=1}^{n} \frac{(f(i;I) - f^{\Delta}(i))^2}{f^{\Delta}(i)} \tag{46}$$

$$f^{\Delta}(i) = \frac{f(i;I) + f(i;J)}{2} \tag{47}$$

$f(i;I)$ and $f^{\Delta}(i)$ represent the observed and expected features, respectively, n n is the number of the bins and $f(i;J)$ represents the feature templates. From Equations (46) and (47), it is deduced that:

$$D(I,J) = \sum_{i=1}^{n} \frac{(f(i;I) - f(i;J))^2}{f(i;I) + f(i;J)} \tag{48}$$

The chi-squared value determines the level of correlation or similarity between any two images and a perfect match is zero while a total mismatch is unbounded.

4. . System Implementation

Figure 3: Canny edge images

The implementation of the models was carried out on Microsoft Windows Vista platform using MATLAB programming language and Java Runtime Environment (JRE) as frontends and PHP as backend on a Pentium IV system with 500GB hard disk and a 4GB RAM. Figure 3 shows some of the results from the Canny edge detection experiments on gray (or RGB) images. Some of the results from the segmentation experiments are also shown in Figure 4 with the detected iris and pupil boundaries shown. Experiments on image cropping were performed for the purpose of isolating the region of interest (white region) from the unwanted region (black region) and typical results are shown in Figure 5 while normalized images of dimension 32 x 280 are shown in Figure 6.

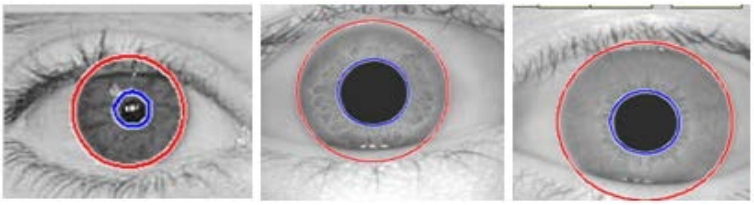

Figure 4: Boundary detections

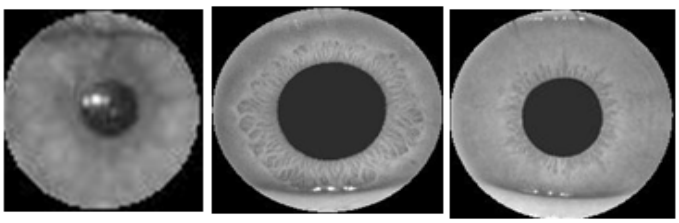

Figure 5: Cropped images

Figure 6: Normalized iris images

A 2D wavelet-based feature extraction from the normalized iris images produced a 4-dimensional feature set representing the horizontal, vertical, diagonal and absolute coefficients. The presence of some eyelid occlusions

or eyelashes in the iris regions and the unequal shape of iris or pupil (which could be elliptical or circular) led to some misleading boundary detections and consequently increased the probability of false rejection. The implementation required changing some of the parameters such as the pupil-search-radius and the iris boundary within the range 9 - 15 and 28 - 60 respectively while fixing Sigma on 0.8 in order to get the most reasonable outcome. Figure 7 is the plot of the distance between two iris images and the number of test samples. The horizontal line starting at distance 2 is the threshold while the points above the threshold line represent the true iris rejected. The false acceptance rate is 0, hence the reason for not appearing on the graph. The application of Independent Component Analysis (ICA) algorithm to the same set of iris image produced an FRR of 1.7391% and FAR of 0% and the plot of the distances of the test iris images is depicted in Figure 8. The system was tested under several environments and recorded 99.94% accuracy with FAR (false acceptance ratio) and FRR (false rejection ratio) of 0.00% and 0.13% respectively. This gives superior performance compared to FRR of 0.87% and 1.03% recorded in [33] and [34] respectively. Tests were conducted on 230 true images and 200 false iris images which recorded 2 rejections and zero acceptances respectively. Collectively, the system recorded an FAR of 0.00% and FRR of 0.869%.

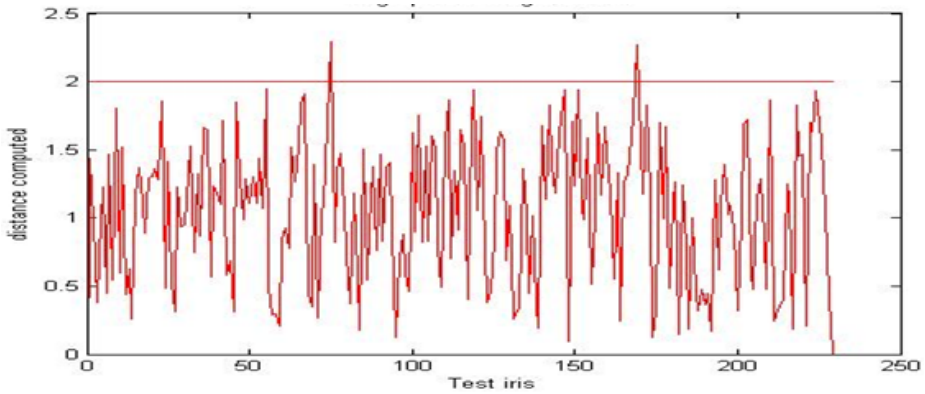

Figure 7: A graph showing the FRR

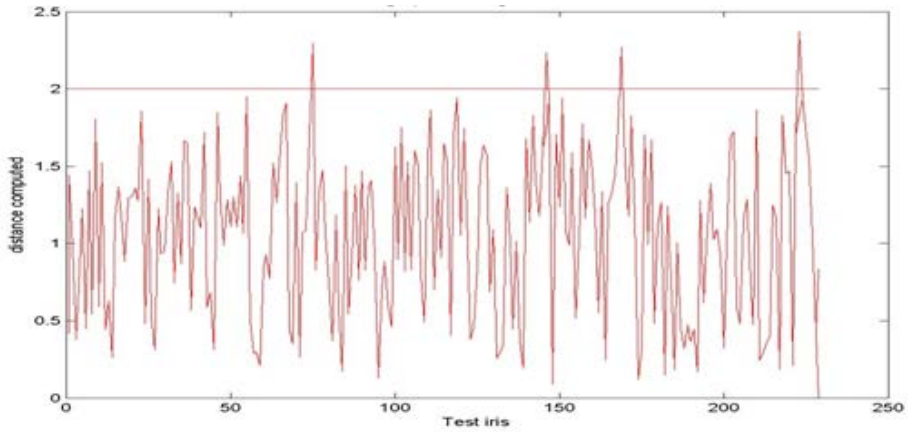

Figure 8: A graph showing FRR

5. .Conclusion

An iris recognition scheme that uses canny edge detection, Hough transform, pseudo-polar coordinate, wavelet transform and chi-square algorithms has been presented. Experimental results showed satisfactory performances

of the scheme when compared with some existing iris recognition systems. It was however noticed that the performance of the system is heavily dependent on the quality of the hardware used for the acquisition of the iris image and there is a limit to which mathematical models can enhance image quality. There are degrading performances in cases of poor quality images and therefore, future work aims at improving the image segmentation and noise removal methods for improved performance.

References

[1] K. Pellerin, Increasing Accuracy in Multimodal Biometric Systems", GIAC Security Essentials Certification (GSEC), SANS Institute (2004). Available: https://www.giac.org/paper/gsec/4110/increasing-accuracy-multimodal-biometric-systems/106587, Accessed 12/03/2014

[2] Q. Jin, X. Tong, P. Ma and S. Bo, "Iris Recognition by New Local Invariant Feature Descriptor", Journal of Computational Information Systems, Vol. 9, No. 5, (2013)

[3] S. Lokhande, V. N. Bapat, "Iris Recognition for Biometric Identification using Wavelet Packet Decomposition", International Journal of Engineering Research & Technology (IJERT), Vol. 1, No. 4, (2012).

[4] M. Devi, "Secure Crypto Multimodal Biometric System for the Privacy Protection of User Identification", International Journal of Innovative Research in Computer and Communication Engineering, Vol.2, Special Issue 1, (2014)

[5] A. K. Jain, L. Hung, S. Pankanti and R. Bolle, "An Identity Authentication System Using Fingerprint", In Proceeding of the IEEE, Vol. 85, (1997), pp. 1365-1388.

[6] D. Prashar, M. Kaur, "Human Eye Iris Recognition Using Discrete 2d Reverse Biorthogonal Wavelet 6.8", International Journal of Scientific & Technology Research Volume 3, Issue 8, (2014)

[7] J. Daugman, "New methods in iris recognition", IEEE Transactions on Systems, Man, and Cybernetics – Part B: Cybernetics, Vol. 37, No. 5, (2007), pp 1167–1175.

[8] M. B. Khan, P. Lavanya "Advanced Secured Vehicle System with Iris Technology and Auto Speed", Advanced Secured Vehicle System with Iris Technology and Auto Speed, Available: http://www.ijedr.org/papers/IJEDR1302018.pdf, Accessed 15/02/2014

[9] H. B. Kekre, D. T. Sudeep, J. Jain, N. Agrawal, "Iris Recognition using Texture Features Extracted from Haarlet Pyramid", International Journal of Computer Applications, Vol. 11, No.12, (2010).

[10] S. M. Matsoso, P. Kuruba, "Iris Recognition Using Circular Hough Transform", International Journal of Innovative Research in Science, Engineering and Technology, Vol. 2, No. 8, (2013).

[11] S. S. Mabrukar, N. S. Sonawane and J. A. Bagban, "Biometric System using Iris Pattern Recognition", International Journal of Innovative Technology and Exploring Engineering, Vol. 2, No. 5, (2013).

[12] E. Rydgren, E. Thomas, F. Amiel, F. Rossant, A. Amara "Iris Features Extraction Using Wavelet Packets", 2004Available:https://static.aminer.org/pdf/PDF/000/320/896/iris_features_extraction_using_wavelet_packets.pdf, Accessed: 23/02/2014.

[13] K. Gaganpreet, A. Girdhar, M. Kaur, "Enhanced Iris Recognition System", International Journal of Computer Applications, Vol. No. 1, (2010).

[14] C. Seung-Seok, S. Yoon, C. Sung-Hyuk and C. C. Tappert "Use of Histogram Distances in Iris Authentication", Available: http://www.csis.pace.edu/~ctappert/srd2004/paper06.pdf, Accessed: 17/08/2014

[15] A. Czajka and A. Pacuta, "Iris Recognition System, Based on Zak-Gabor Wavelet Packets", Journal of Telecommunications and Information Technology, Available: http://citeseerx.ist.psu.edu/viewdoc/download?doi=10.1.1.469.3897&rep=rep1&type=pdf, Accessed: 23/01/2014

[16] Z. W. Yao, Z. Jun, W. Y. Feng and W. M. Jun, "Iris Feature Extraction based on Haar Wavelet Transform", International Journal of Security and Its Applications, Vol. 8, No. 4 (2014), pp. 265-272

[17] G. A. Panganiban, N. B. Linsangan and F. S. Caluyo, "Implementation of Wavelet Transform-Based Algorithm for Iris Recognition System", International Journal of Information and Electronics Engineering, Vol. 2, No. 3, (2012)

[18] A. Azizi, H. R. Pourreza, "Efficient IRIS Recognition Through Improvement of Feature Extraction and subset Selection", International Journal of Computer Science and Information Security, Vol. 2, No. 1, (2009)

[19] Y. Du, C. Belcher and Z. Zhou, "Scale Invariant Gabor Descriptor-Based Non-cooperative Iris Recognition", EURASIP Journal on Advances in Signal Processing, Vol. 2010, Available: http://asp.eurasipjournals.com /content/2010/1/936512

[20] S. Lokhande and V. N. Bapat, "Wavelet Packet Based Iris Texture Analysis for Person Authentication", Signal & Image Processing: An International Journal (SIPIJ) Vol. 4, No. 2, (2013)

[21] X. He and P. Shi, "Extraction of Complex Wavelet Features for Iris Recognition", Proceedings of 19th International Conference on Pattern Recognition, 8-11 Dec. 2008, Tampa, FL (2008)

[23] S.Hariprasath and V.Mohan, "Iris Pattern Recognition Using Complex Wavelet and Wavelet Packet

Transform", Journal of Computer Applications, Vol. 2, No.2, (2009)

[24] K. A. Khobragade, K. V. Kale, "Multi-wavelet based Feature Extraction Algorithm for Iris Recognition", International Journal of Engineering and Innovative Technology (IJEIT) Volume 3, No. 12, (2014)

[25] P. Dhankhar, N. Sahu, "A Review and Research of Edge Detection Techniques for Image Segmentation", International Journal of Computer Science and Mobile Computing (IJCSMC), Vol. 2, No. 7, (2013), pp. 86 – 92

[26] C.M.Patil, S. Patilkulkarani, "An Approach of Iris Feature Extraction for Personal identification", Proceedings of International Conference on Advances in Recent Technologies in Communication and Computing, 27-28 Oct. 2009, Kottayam, Kerala, pp. 796 – 799.

[27] B. Li, U. Söderström, S. U. Réhman, H. Li, "Restricted Hysteresis Reduce Redundancy in Edge Detection", Journal of Signal and Information Processing, Vol. 4, (2013), pp 158-163.

[28] J. Canny, "A Computational Approach to Edge Detection", IEEE Transactions on Pattern Analysis and Machine Intelligence, Vol. 8, No. 6, (1986).

[29] N. S. Sharma, R. Sharma, "Comparison Between Circular Hough Transform And Modified Canny Edge Detection Algorithm For Circle Detection", International Journal of Engineering Research & Technology (IJERT) Vol. 1 No. 3, (2012).

[30] D. Ioannou, W. Huda, A. F. Laine, "Circle recognition through a 2D Hough Transform and radius histogramming", Image and Vision Computing, Vol. 17, (1999), pp. 15–26

[31] F. Dembele, "Object detection using Circular Hough Transform", Available: http://wcours.gel.ulaval.ca/ 2015/a/GIF7002/default/5notes/diapositives/pdf_A15/lectures%20supplementaires/C11d.pdf, Accessed: 21/03/2014.

[32] J. Daugman, "High confidence visual recognition of persons by a test of statistical independence", IEEE Trans. PAMI, vol. PAMI-15, (1999), pp. 1148-1161

[33] L. Ma, T. Tan, Y. Wang, D. Zhang "Personal Identification Based on Iris Texture Analysis", IEEE Transactions on Pattern Analysis and Machine Intelligence, Vol. 25, No. 12, (2003), pp. 1519- 1533

[34] T. Tan, L. Ma, Y. Wang and D. Zhang "Personal Identification based on Iris Texture Analysis", IEEE Transactions on Pattern Analysis and Machine Intelligence, Vol. 25, No. 12, (2003), pp. 1519-1533.